Raman spectroscopy and biomarker analysis reveal multiple carbon inputs to a Precambrian glacial sediment

Alison Olcott Marshall, Frank A. Corsetti, Alex L. Sessions, Craig P. Marshall

PII: S0146-6380(09)00186-7
DOI: 10.1016/j.orggeochem.2009.08.006
Reference: OG 2390

To appear in: *Organic Geochemistry*

Received Date: 22 April 2009
Revised Date: 19 August 2009
Accepted Date: 25 August 2009

Please cite this article as: Marshall, A.O., Corsetti, F.A., Sessions, A.L., Marshall, C.P., Raman spectroscopy and biomarker analysis reveal multiple carbon inputs to a Precambrian glacial sediment, *Organic Geochemistry* (2009), doi: 10.1016/j.orggeochem.2009.08.006

Raman spectroscopy and biomarker analysis reveal multiple carbon inputs to a Precambrian glacial sediment

Alison Olcott Marshall [a*], Frank A. Corsetti [b], Alex L. Sessions [c], Craig P. Marshall [a]

[a] *Department of Geology, University of Kansas, Lawrence, KS 66045 USA*

[b] *Department of Earth Sciences, University of Southern California, Los Angeles, CA 90089, USA*

[c] *Division of Geological and Planetary Science, California Institute of Technology, Pasadena, CA 91125, USA*

[*]-Corresponding Author. Tel: +1.785.864.1917; fax: +1.785. 864.5276.

E-mail address: olcott@ku.edu. (Alison Olcott Marshall).

ABSTRACT

Extractable biomarkers can elucidate the environment and biota of ancient glaciations, although the method must be applied with care, as glacial sediments have a potential for incorporation of older detrital carbon. In Phanerozoic glacial sediments, the distinct elemental, molecular and isotopic compositions of the terrestrial and marine biomass allow discrimination between primary marine and redeposited terrestrial organic matter. However, as the Proterozoic biosphere was largely microbial and marine, biomarker and isotopic analyses are insufficient for distinguishing primary organic matter from secondary reworked organic matter. Here, we report the

combined application of Raman spectroscopy and biomarker analysis to Precambrian glacial sediments, which, together, allow discrimination between mixed pools of organic carbon and provide a promising new approach for rapidly screening Precambrian sediments for immature organic matter amenable to biomarker analysis.

Keywords: Raman Spectroscopy; biomarker; glaciation; Precambrian; detrital organic matter; Snowball Earth

1. Introduction

Geologic, paleomagnetic and geochemical evidence record two of the most severe glaciations in the Earth's history during the Neoproterozoic (ca. 750 and 630 Ma, the so-called "Snowball Earth" periods), with glaciation so extreme that ice was present at equatorial latitudes (Evans, 2000; Kirschvink, 1992; Kirschvink et al., 2000). However, there is no geological observation that can indicate how thick the ice was during a glacial event, and consequently the severity of the impact on the biota. Thus, while numerous scenarios have been proposed to explain the Neoproterozoic glacial sediments (e.g. Grotzinger and Knoll, 1995; Hoffman and Schrag, 2002; Hoffman et al., 1998; Kennedy et al., 2001), including those denying that a glaciation even occurred (Eyles and Januszczak, 2003), no one hypothesis is supported or excluded by all of the data. Furthermore, while there have been

multiple examinations of microfossil assemblages before and after the glaciations (Corsetti et al., 2003; Grey et al., 2003; Knoll, 1985; Leiming and Xunlai, 2007; Moczydłowska, 2008; Nagy et al., 2009), the microfossil record during the glaciation is too sparse to preserve the effect these low-latitude glaciations had on the biosphere. In the Proterozoic, as in the Phanerozoic, biomarkers offer a potentially powerful tool for understanding such ancient glacial environments and their environmental impact (Olcott et al., 2005). However, in applying these tools to glacial sediments, the potential for incorporation of older detrital organic matter (OM) must be carefully considered. Geochemical studies of Quaternary glaciations have documented that marine glaciogenic sediments contain both primary marine OM and redeposited terrestrial material transported by glaciers (e.g. Fabianska et al., 2008; McDonald et al., 1991; Villanueva et al., 1997). Marine biomass and terrestrial arboreal biomass have distinct elemental, molecular and isotopic compositions, enabling them to be clearly distinguished in most Phanerozoic deposits. However, the Proterozoic biosphere was primarily microbial and marine, so biomarker and isotopic studies alone are unable to distinguish contemporary vs. ancient sources of organic material preserved in glacial sediments.

Here, we report the combined application of Raman spectroscopy and biomarker analysis to a study of Precambrian glacial sediments from the

Vazante Group of Brazil. The data allow elucidation of mixed pools of organic carbon and provide a promising new approach for rapidly screening Precambrian sediments for thermally immature OM amenable to biomarker analysis.

2. The Vazante Group, São Francisco Craton, Brazil

The Vazante Basin is located in the northwestern part of Minas Gerais, on the São Francisco Craton. The craton is composed of Archean and Paleoproterozoic basement rocks covered by Meso- and Neoproterozoic sedimentary sequences. The current geometry of the basin is thought to result from the Brazilian-Pan African orogeny, which culminated ca. 600-500 Ma (Azmy et al., 2001; Fig. 1). More than 300,000 km^2 of Neoproterozoic sediments exist on the craton (Azmy et al., 2001). Sediments of the Vazante Group outcrop over ca. 10,000 km^2, but are generally too highly metamorphosed for organic geochemical studies (Babinski et al., 2005). However, some subsurface samples have been drilled, which exhibit only slight metamorphism (Azmy et al., 2001, 2006). Seven separate formations are recognized within the Vazante Group (from oldest to youngest): Santo Antônio do Bonito, Rocina, Lagamar, Serra do Garrote, Serra do Poço Verde, Morro do Calcário and Lapa.

The Vazante Group was first recognized as glaciogenic by Derby (1888), although its age has long been contentious. On the basis of lithology and chemostratigraphy, many researchers identify the sediments as Neoproterozoic (Babinski et al., 2005; Olcott et al., 2005), although some have proposed an older age, ca. 1000 Ma, on the basis of stromatolite biostratigraphy (Cloud and Dardenne, 1973) and Re-Os chronometry (Azmy et al., 2008). Regardless of age, the Lapa Formation is recognized as a post-glacial, cap carbonate, while the Serra do Garrote, Serra do Poço Verde, and Morro do Calcário formations are all syn-glacial and contain glaciogenic lithologies such as diamictite and lonestones. In 2002, we sampled the Serra do Poço Verde Formation from core MAF 42-88, originally recovered in 2000 at 17°29'49" S, 46°49'49" W by the Brazilian mining company Votorantim. Samples were collected from a black shale unit, as well as the flanking diamictic and carbonate marl units (Fig. 2). Thin sections of samples from the black shale unit reveal finely disseminated OM, as well as abundant pyrite and glendonite, a pseudomorph of the hydrated low temperature carbonate ikaite (Fig. 3). Glendonite is viewed as an indication that fresh OM was buried, as the formation of ikaite is thought to require both cold temperatures and the rapid remineralization of OM to elevate dissolved inorganic carbon (DIC; Suess et al., 1982). Ikaite nodules must have formed soon after deposition, because they preserve uncompacted laminations (Fig.

3b). In contrast, thin sections from the carbonate units flanking the black shale contain little OM or pyrite (Fig. 3c).

3. Methods

3.1. Raman spectroscopy

Standard petrographic thin sections were analyzed using Raman spectroscopy. Spectra were collected at several different locations in multiple thin sections using a Renishaw InVia Reflex Raman Microprobe with charge-coupled detector. The collection optics are based on a Leica DMLM microscope. A refractive glass 50 x objective lens was used to focus the laser to a 2 μm spot to collect backscattered radiation. The 514.5 nm line of a 5 W Ar+ laser (Spectra-Physics Stabilite 2017 laser) orientated normal to the sample and to the laminations in the shale was used to excite the sample. Surface laser power settings of 1.0–1.5 mW were used to minimize laser induced heating of the OM. Such heating can be readily detected as a downward shift in the G band to 1565 cm^{-1}, which was not observed for any of the spectra acquired. Each spectrum was acquired using 10 scans and an accumulation time of 30 s, which gave good signal-to-noise ratio. Scan ranges were 1000-1800 cm^{-1} in the carbon first-order region and whole spectral region scans 100-4000 cm^{-1} were also collected. Multiple analyses were performed on each thin section on carbon clots a few mm away from one another.

3.2. Biomarker analysis

Samples for biomarker analysis were processed one at a time to avoid cross-contamination. Ca. 30 g of rock were washed in distilled water. Samples were air-dried at room temperature and crushed to <5 cm pieces with a jaw-type rock crusher whose exposed surfaces had been cleaned (4 x) with acetone and then dichloromethane (DCM). The pieces were sonicated in 9:1 DCM:MeOH for 2 min and crushed again to <1 cm with a smaller rock crusher cleaned as before. The ultrasonic extraction was repeated, and the sample was powdered in a shatterbox that had been cleaned using grinding quartz sand followed by acetone and DCM rinses (4 x). The powdered rock was extracted in a microwave accelerated reaction system (MARS Express, CEM Corp.) as follows: 20 g rock powder were split equally between 5 clean Teflon vessels; 25 ml of 9:1 DCM/MeOH was added to each, and the samples were extracted at 100 °C for 15 min with stirring. Extracts were filtered through combusted glass fiber filters to remove particulates and solvent was evaporated to ca. 30 ml under N_2 at 35 °C, taking care not to allow them to completely dry out. Elemental S was removed by filtration through activated Cu and the S°-free extract was evaporated to near dryness under N_2. Silica gel column chromatography was used to separate the extracts into aliphatic and aromatic fractions. The aliphatic fraction was transferred to a vial with hexane; the solvent volume was reduced under N_2 to 50 µl and the fraction

analyzed using gas chromatography/mass spectrometry (GC/MS). Hexadecanoic acid isobutyl ester was added to all samples as an internal standard. Extracts from the two intermediate stages of crushing were prepared and analyzed following the same procedures. All samples were analyzed with a ThermoFinnigan Trace GC-DSQ quadrupole MS equipped with a DB-5MS column (30 m x 0.25 mm, 0.25 μm film thickness). Aliquots (1 μl) were injected using a PTV injector (35 °C for 3 min, 14.5 °C/s ramp to 200 °C, then 12 °C/s ramp to 350 °C (held 3 min). The column oven was programmed at 20 °C/min ramp to 130 °C, then 5°C/min ramp to 320 °C (held 20 min).

Laboratory blanks of all materials used in the laboratory procedures, including the solvents, Cu, silica gel and MARS vessels, were analyzed via GC/MS. No hydrocarbons, oil residues or unresolved complex mixtures (UCMs) were observed. In addition, a block of basalt was baked overnight at 450 °C and spiked with a standard hydrocarbon solution and subjected to the entire analytical procedure, no contaminants again being detected. Biomarker yields were confirmed with replicate extractions of duplicate samples.

3.3. H/C analysis

Kerogen was isolated by agitation in HCl and HF for two days and ca. 2 mg were weighed into a tin sample boat. The elemental H and C contents were determined using a Perkin-Elmer 2400 Elemental Analyzer (the H/C ratio values were measured by the commercial lab Baseline Resolution, Shenandoah, Texas, USA; Table 1).

4.. Results

4.1. Raman spectroscopy

Representative carbon first-order Raman spectra are presented in Fig. 2. Samples from the black shale unit, at 805, 812, 816 and 817 m, and two from the carbonate marl unit (759 m) are marked by a sloping baseline because of fluorescence radiation overlying weak Raman lines. The spectra from 812, 816 and 817 m also contain weak bands on a sloping baseline at ca. 1650 cm^{-1}, ca. 1600 cm^{-1} and ca. 1350 cm^{-1}. The samples from the carbonate marl unit (783 m and two of the three samples from 759 m) and from the diamictite unit (858 m) are marked by distinct bands at ca. 1600 cm^{-1} and ca. 1350 cm^{-1}. The Raman spectrum of an ideal graphite crystal (space group D^4_{6h} with unlimited translational symmetry) contains only one first order band, at 1580 cm^{-1}. This 'G' band corresponds to an ideal graphitic lattice vibrational mode with E_{2g} symmetry (Tuinstra and Koenig, 1970). Disordered carbonaceous material also displays bands characteristic of disordered sp^2 carbon. The size of these 'D' bands decreases relative to the G band as more order is

introduced to the carbonaceous structure, e.g. during metamorphism (Jehlička and Beny, 1999). The most intense band (D1) is at 1350 cm^{-1}, corresponding to a disordered lattice vibration mode with A_{1g} symmetry. The D2 band is observable as a shoulder on the G band at 1620 cm^{-1} and corresponds to a graphitic lattice mode with E_{2g2} symmetry (Dresselhaus and Dresselhaus, 1981). Carbonate-rich samples from both the black shale unit and the diamictite also produce a band at ca. 1066 cm^{-1} assigned to the ν_1 symmetric CO_3^{-} stretching mode. Samples from 759 and 805 m were each scanned at multiple locations in the individual thin sections. While the sampled organic carbon blebs were located only cm apart, the resulting spectra differ markedly (Fig. 2).

The full region Raman spectra from samples representing both carbonate and black shale units are quite different from one another (Fig. 4). The carbonate marl sample at 783 m is marked by three distinct bands at 2700-3200 cm^{-1}. These are assigned to second-order carbon bands denoted as S_i between 2700 and 3300 cm^{-1}. They result from overtone scattering (2 × 1360 = 2720 cm^{-1}, the most intense, and 2 × 1620 = 3240 cm^{-1}, a weak but sharp band) and combination scattering (1620 + 830 = 2450 cm^{-1}, 1580 + 1355 = 2935 cm^{-1}). The appearance of three dimensional ordering in disordered sp^2 carbonaceous materials is observed with overtone and combination bands of the G and D bands assigned to the S band. Samples from the black shale unit (805, 812

and 816 m) instead have a moderate band at 2700-3000 cm^{-1}, assigned to aliphatic C-H_x stretching modes on a sloping baseline. There are also significant variations between the two different spectra from 805 m.

Raman bands observed in the carbonate samples at 783 and 858 m, and in two of the three spectra at 759 m, are attributed to the D1 band at ca. 1350 cm^{-1}, and a combination of the G and D2 bands at ca. 1650cm^{-1}. While D1, G, and D2 bands are visible for the black shale samples from 812, 816 and 817 m, the band at ca. 1650 cm^{-1} is indicative of ν(C=O) while that at 1470-1435 cm^{-1} is due to the aliphatic deformational mode δ(C-H). A vibrational stretching mode for aliphatic ν(C-H_x), distinct from the S band, can be observed between 2700 and 3000 cm^{-1} in the full region scan of samples from 805, 812 and 816 m. Finally, the bands at ca. 1066 cm^{-1} visible for many samples are due to ν_1 symmetric CO_3^- stretching mode of carbonates.

4.2. GC/MS

Total ion chromatograms (TICs) for all the samples are presented in Fig. 2. The most abundant compounds in all the extracts are long chain *n*-alkanes, but the distribution varies (Fig. 2). While the extraction procedure does not recover *n*-alkanes lighter than ca. C_{17}, samples from within black shale units (805-817 m) are dominated by low molecular weight (LMW) compounds, with the most abundant *n*-alkane <*n*-C_{26}. In contrast, samples extracted from

carbonate marls (759 and 783m) and the diamictite-rich carbonate unit (858 m) are dominated by higher molecular weight (HMW) *n*-alkanes, with the most abundant at ca. *n*-C_{30}.

Hopanes from C_{29}-C_{32}, dominated by the C_{29} *αβ* and C_{30} *αβ* hopanes, were detected in all the black shale samples, but not in samples from the diamictite (858 m) or from carbonate marls (759 and 783 m; Fig. 5). Similarly, C_{27}-C_{29} steranes, dominated by the C_{27} 20*R* *ααα* sterane, were detected in allthe black shale samples but not in the diamictite or marl samples (Fig. 5).

4.3. H/C values and extract yields

The H/C values vary widely (Table 1). They range from 0.68 at 812 m to 0.29 at 783 m. The extract yields also range widely, from 2.4 μg/g rock at 858 m to 13.5 μg/g rock at 817 m (Table 1).

5. Discussion

5.1. Raman spectra

The Raman spectra of the carbonate marl at 783 and 759 m and the diamictite sample at 858 m indicate thermally mature organic carbon. Both the presence of evolved D and G bands, indicating disordered sp^2 carbon, and the presence of overtone bands in the full region scan of the sample at 783 m,

are consistent with this conclusion. The spectra are similar to those of other mature samples that have undergone greenschist metamorphic alteration (Beyssac et al., 2002, 2003; Jehlička and Beny, 1999; Jehlička et al., 2003; Marshall et al., 2007). However, the carbon in the samples is not uniformly mature. For example, analysis of different clots of carbon in one thin section of the marl reveal a continuum of maturity (cf. three spectra for 759 m in Fig. 2). While the Raman spectrum of one carbon bleb in the thin section from 759 m contains evolved D and G bands, similar to those seen in the other two carbonate samples, another carbon bleb a few cm away contains slight D and G bands on a sloping baseline, indicative of fluorescence from saturated C-H bonds producing an electronic effect with a longer lifetime than the Raman effect (Marshall et al., 2006; Fig 2). A third carbon bleb in this thin section is of sufficient aliphatic character that the baseline fluorescence swamps any other bands. This aliphatic character suggests organic carbon that has not seen thermal alteration above ca. 200 °C (Jehlička and Beny, 1999). Thus, Raman spectra from the sample at 759 m indicate that the kerogen contained within a single thin section has a range of maturity.

All of the kerogen clots from the black shale unit, including two from a thin section at 805 m, have baseline fluorescence resulting from saturated C-H aliphatic bonds. While the samples at 816 and 817 m have D and G bands, they also have a band at 1650 cm^{-1}, indicative of C=O bonds. This latter

feature suggests that the sample has not undergone a high degree of thermal alteration, as the C=O structure is not preserved at high temperature (Brocks and Summons, 2003). Alternatively, D and G Raman bands in these samples could arise from an immature kerogen with an unusual aromatic nature containing C=O bonds, rather than from a lack of thermal alteration. Regardless, the immaturity of the samples is further supported by the full region Raman spectra which contain evidence of abundant C-H bonds. While the two analyses of the black shale from 805 m do not show the same range of heterogeneity as the marl samples from 759 m, the two samples at 805 m do have different full region spectra, with one area showing evidence for C=O and C-H bonds, while the other does not.

The variability in maturity indicated by the Raman data is too large and at too small a scale (<1 mm) to be explained by regional metamorphism or even local hydrothermal alteration (Jehlička and Beny, 1992). Rather, we attribute the observed variations in the spectra to multiple generations of organic carbon within the rocks. Kerogen containing evidence for carbonyl groups and aliphatic C-H bonds is immature and presumably derived from fresh OM buried with the sediments, whereas kerogen with more highly ordered structure is older, mature, and probably represents detrital material eroded and transported by the glaciers.

5.2. Extractable biomarkers

The distribution of *n*-alkanes is also quite different between black shales and carbonates, with the black shale samples dominated by LMW *n*-alkanes, while the carbonate samples are dominated by HMW *n*-alkanes. In a study of Quaternary glacial sediments, a similar pattern was seen between samples containing redeposited and fresh OM (Fabianska et al., 2008). In samples containing mainly reworked mature organic carbon, *n*-alkanes were dominated by HMW compounds, while in samples containing more fresh (i.e., synglacial) organic carbon the *n*-alkanes were predominately LMW compounds (Fabianska et al., 2008). However, the high maturity indicated for some kerogens is likely inconsistent with the preservation of even HMW *n*-alkanes, so it is possible that the HMW *n*-alkane envelope in carbonate samples represents trace contamination, a common problem for Precambrian samples (Sherman et al., 2007).

Hopanes and steranes were detected above background only in samples from black shale units (i.e. those containing LMW *n*-alkanes and producing Raman spectra indicative of the least mature kerogen). Unlike *n*-alkanes, which are ubiquitous and not indicative of a specific biologic input, hopanes and steranes are indicative of bacterial and algal inputs, respectively (Ourisson and Albrecht, 1992; Volkman, 2003). Like the *n*-alkanes, these compounds are generally not preserved at temperatures above ca. 200 ^{o}C and have never

been reliably detected in rocks reaching Greenschist facies metamorphism [Brocks and Summons, 2003 (hydrocarbons in fluid inclusions are an exception; see Dutkiewicz et al., 2006; George et al., 2007, 2009)]. While contamination must be considered a possibility, its abundance is uncorrelated with the appearance of HMW *n*-alkanes, so two separate and distinct sources of contamination would have to be postulated. Thus the hopane and sterane biomarkers are most plausibly interpreted as being associated with the low-temperature kerogen in black shale samples.

5.3. Elemental H/C values

The H/C ratio of kerogen is often used as an indicator of maturity, with thermal alteration preferentially removing H and leading to lower H/C values of kerogen. In general, H/C values >0.5 are taken to be representative of rocks heated to less than ca. 200 °C (Hayes et al., 1983). The variance in HC values of our samples occurs over too short a distance to be attributed to regional metamorphism or local hydrothermal alteration. However, the result can be readily explained by the presence of two (or more) generations of kerogen, with differing H/C values and different mixing ratios in different strata. While the varying H/C ratio values cannot prove our hypothesis, the presence of values as high as 0.68 is consistent with there being a significant component of immature kerogen in the rocks.

5.4. Carbon inputs to glacial sediments

Studies of modern marine glacial sediments, analyzed for the presence of terrestrial debris, extractable compounds derived from aquatic and terrestrial organisms and biomarker maturity ratios indicative of eroded petrogenic organic carbon, have revealed that recent glaciations typically contain three populations of OM: marine, terrestrial and reworked petrogenic organic carbon (Fabianska et al., 2008; McDonald et al., 1991; Schouten et al., 2007; Villanueva et al., 1997). However, in the Precambrian there was not a significant terrestrial biota. While there is some evidence for Proterozoic fungi (Butterfield, 2005) and lichen (Yuan et al., 2005), these seem to have dwelt in shallow marine settings, not on the land. Thus, it is reasonable to suppose that these glacial sediments contain only two different sources of organic carbon: synglacial marine OM and redeposited older, more thermally mature, organic carbon originating from black shales in the source region and transported to the marine basin during glaciation. In carbonate units, the older, more mature organic carbon seems to represent a majority of the organic carbon. Not only do the Raman data reveal that most of the organic carbon within these units is mature, but there are no preserved diagnostic biomarkers, only HMW *n*-alkanes. In contrast, within the black shale samples, it seems as if much of the organic carbon is immature, and thus likely representative of fresh primary production. The majority of the Raman spectra are indicative of immature carbon and there are extractable

biomarkers indicative of bacterial and algal inputs. The geological data are also consistent with a large degree of primary organic input: these samples are more organic rich than the carbonate samples and the presence of glendonite indicates that OM was rapidly remineralized after deposition.

6. Significance for Snowball Earth

Neoproterozoic low-latitude glaciations are widely assumed to produce drastic effects in the biosphere (e.g. Hoffman et al., 1998; Runnegar, 2000; Schrag and Hoffman, 2001), the assumptions being based primarily on the carbon isotopic record of post-glacial successions. While the available fossil record is not robust enough to assess the state of the biosphere during these glaciations, biomarkers offer a potentially powerful tool for understanding ancient glacial environments and their biota (Elie et al., 2007; Olcott et al., 2005).

A previous study (Olcott et al., 2005) of the extractable biomarkers preserved within the synglacial Vazante Formation concluded that they indicate a complex and productive ecosystem, comprised of both photosynthetic and heterotrophic bacteria as well as eukaryotes. The data were then used to argue that the Sturtian glaciation did not, at this locality, produce a dramatic decline in marine productivity. The relevance of that study for Snowball glaciations was subsequently questioned by Azmy et al. (2008), because Re-

Os dates for rocks from the same formation suggested ages of ca.1000 Ma, significantly older than Sturtian glaciations. However, Re-Os dating relies on the relative proportion of hydrogenous Re and Os associated with organic carbon within black shales and is highly sensitive to the presence of non-hydrogenous, inherited Re and Os (Ravizza and Turekian, 1989; Ravizza et al., 1991; Selby and Creaser, 2003). For example, 8000 yr old sediments in the Black Sea, which has a high rate of deposition of detrital material, yield Re-OS dates of 12 ± 5 Ma (Ravizza et al., 1991).

Given that our new data now strongly suggest that glaciogenic rocks of the Vazante Formation contain both fresh and detrital organic carbon, the interpretation of ca. 1000 Ma Re-Os dates for the Vazante must be reconsidered. It is possible, perhaps even likely, that those dates represent the weighted mean of the two generations of carbon contained in the Vazante black shales. This interpretation is consistent with the observation that Mean Standard Weight Deviations on the isochrons for these samples are quite high (65) when compared with those of other Neoproterozoic glacial successions (e.g. 1.1 on the Australian Tildelpina Shale; Azmy et al., 2008; Kendall et al., 2006). Furthermore, Vazante Fm shales contain detrital zircons with a large scatter in ages, ranging from the Archean to the Mesoproterozoic, also suggestive of allochthonous input (Azmy et al., 2008). Thus, the timing of deposition of these rocks with respect to global glaciation

remains uncertain.

7. Conclusions

Raman spectral analysis of kerogen contained within glacial deposits on the São Francisco craton in Brazil reveals that the rocks contain at least two generations of kerogen, one of low maturity and aliphatic character, the other more structurally ordered and of high maturity. This conclusion is supported by extractable biomarker data, with hopane and sterane abundance highly correlated with rocks showing Raman spectra indicative of low maturity. In contrast, samples containing mostly mature organic carbon contain only HMW *n*-alkanes and no hopanes or steranes.

Given that most glaciogenic sediments are likely to contain multiple generations of OM, extreme care must be taken in the application of techniques which rely on bulk measurements of organic carbon, including whole-rock $\delta^{13}C$, H/C and Re-OS geochronology. Raman spectroscopy with μm scale spatial resolution has proven to be a valuable approach for identifying and distinguishing multiple generations of kerogen and could serve as a valuable tool for rapid screening of rocks prior to laborious biomarker analysis.

Acknowledgements

We thank the Votorantim Metais company and T. F. de Oliveira for samples and the Australian Research Council and a NSF grant (EAR0418083) for funding, as well as J. Jehlička and an anonymous reviewer for constructive comments.

Associate Editor – **S. Schouten**

References

Azmy, K., Kaufman, A., Misi, A., de Oliveira, T., 2006. Isotope stratigraphy of the Lapa Formation, São Francisco Basin, Brazil: Implications for Late Neoproterozoic glacial events in South America. Precambrian Research 149, 231-248.

Azmy, K., Kendall, B., Creaser, R., Heaman, L., de Oliveira, T., 2008. Global correlation of the Vazante Group, São Francisco Basin, Brazil: Re–Os and U–Pb radiometric age constraints. Precambrian Research 164, 160-172.

Azmy, K., Veizer, J., Misi, A., de Oliveira, T.F., Sanches, A.L., Dardenne, M.A., 2001. Dolomitization and isotope stratigraphy of the Vazante Formation, Sao Francisco Basin, Brazil. Precambrian Research 112, 303-329.

Babinski, M., Monteiro, L., Fetter, A., Bettencourt, J., de Oliveira, T., 2005. Isotope geochemistry of the mafic dikes from the Vazante nonsulfide

zinc deposit, Brazil. Journal of South American Earth Sciences 18, 293-304.

Beyssac, O., Goffe, B., Chopin, C., Rouzaud, J.N., 2002. Raman spectra of carbonaceous material in metasediments: a new geothermometer. Journal of Metamorphic Geology 20, 859-871.

Beyssac, O., Goffe, B., Petitet, J.-P., Froigneux, E., Moreau, M., Rouzaud, J.-N., 2003. On the characterization of disordered and heterogeneous carbonaceous materials by Raman spectroscopy. Spectrochimica Acta Part A: Molecular and Biomolecular Spectroscopy 59, 2267.

Brocks, J., Summons, R., 2003. Sedimentary hydrocarbons, biomarkers for early life. Treatise on Geochemistry 8, 63-115.

Butterfield, N., 2005. Probable Proterozoic fungi. Paleobiology 31, 165-182.

Cloud, P.E., Dardenne, M.A., 1973. Proterozoic age of the Bambui Group in Brazil. Geological Society of America Bulletin 84, 1673–1676.

Corsetti, F., Awramik, S., Pierce, D., 2003. A complex microbiota from snowball Earth times: microfossils from the Neoproterozoic Kingston Peak Formation, Death Valley, USA. Proceedings of the National Academy of Sciences USA 100, 4399-4404.

Derby, D.A., 1888. Uber dui spuren einen carbonen vereisung in Sudamerika. Neues Jahrbuch fur Mineralogie, Geologie und Palaeontologie 188, 172-176.

Dresselhaus, M.S., Dresselhaus, G., 1981. Intercalation compounds of graphite. Advances in Physics 302, 139-326.

Dutkiewicz, A., Volk, H., George, S.C., Ridley, J., Buick, R., 2006. Biomarkers from Huronian oil-bearing fluid inclusions: An uncontaminated record of life before the Great Oxidation Event. Geology 34, 437-440.

Elie, M., Nogueira, A.C.R., Nedelec, A., Trindade, R., 2007. A red algal bloom in the aftermath of the Marinoan Snowball Earth. Terra Nova 19, 303-308.

Evans, D.A.D., 2000. Stratigraphic, geochronological, and paleomagnetic constraints upon the Neoproterozoic climatic paradox. American Journal of Science 30, 347-433.

Eyles, N., Januszczak, N., 2003. 'Zipper-rift': a tectonic model for Neoproterozoic glaciations during the breakup of Rodinia after 750 Ma. Earth-Science Reviews 65, 1-73.

Fabianska, M., Miotlinski, K., Kowalczyk, A., 2008. Geochemical features of re-deposited organic matter occurring in fluvioglacial sediments in the Racibórz region Poland: A case study. Chemical Geology 25, 151-161.

George, S.C., Dutkiewicz, A., Herbert, V., Ridley, J., 2009. Oil-bearing fluid inclusions from the Palaeoproterozoic: A review of biogeochemical results from time-capsules >2.0 Ga old. Science in China, Series D: Earth Sciences 52, 1-11.

George, S.C., Volk, H., Dutkiewicz, A., Ridley, J., Buick, R., 2008. Preservation of hydrocarbons and biomarkers in oil trapped inside fluid inclusions for >2 billion years. Geochimica et Cosmochimica Acta 72, 844-870.

Grey, K., Walter, M.R., Calver, C.R., 2003. Neoproterozoic biotic diversification: Snowball Earth or aftermath of the Acraman impact? Geology 31, 459-462.

Grotzinger, J., Knoll, A., 1995. Anomalous carbonate precipitates: Is the Precambrian the key to the Permian? Palaios 10, 578-596.

Hayes, J.M., Kaplan, I.R., Wedeking, K.W., 1983. Precambrian organic geochemistry, preservation of the record. In: Schopf, J.W. (Ed.), Earth's Earliest Biosphere: Its Origin and Evolution,Princeton University Press, Princeton, NJ, pp. 93-134.

Hoffman, P.F., Kaufman, A., Halverson, G.P., Schrag, D.P., 1998. A Neoproterozoic snowball earth. Science 281, 1342-1346.

Hoffman, P.F., Schrag, D., 2002. The snowball Earth hypothesis: testing the limits of global change. Terra Nova 14, 129-155.

Jehlička, J., Beny, C., 1992. Application of Raman microspectrometry in the study of structural changes in Precambrian kerogens during regional metamorphism. Organic Geochemistry 18, 211-213.

Jehlička, J., Beny, C., 1999. First and second order Raman spectra of natural highly carbonified organic compounds from highly metamorphic rocks. Journal of Molecular Structure 480/481, 541-545.

Jehlička, J., Urban, O., Pokorný, J., 2003. Raman spectroscopy of carbon and solid bitumens in sedimentary and metamorphic rocks. Spectrochimica Acta Part A 59, 2341-2352.

Kendall, B., Creaser, R., Selby, D., 2006. Re-Os geochronology of postglacial black shales in Australia: Constraints on the timing of "Sturtian" glaciation. Geology 34, 729.

Kirschvink, J.L., 1992. Late Proterozoic low-latitude global glaciation; the snowball Earth. In: J.W. Schopf, C. Klein (Eds.), The Proterozoic Biosphere; a Multidisciplinary Study. Cambridge Press, Cambridge. pp. 1348.

Kirschvink, J.L., Gaidos, E.J., Bertani, L.E., Beukes, N.J., Gutzmer, J., Maepa, L.N., Steinberger, R.E., 2000. Paleoproterozoic snowball Earth; extreme climatic and geochemical global change and its biological consequences. Proceedings of the National Academy of Sciences USA 974, 1400-1405.

Knoll, A.H., 1985. The distribution and evolution of microbial life in the Late Proterozoic era. Annual Review of Microbiology 39, 391-417.

Leiming, Y., Xunlai, Y., 2007. Radiation of Meso-Neoproterozoic and Early Cambrian protists inferred from the microfossil record of China. Palaeogeography, Palaeoclimatology, Palaeoecology 254, 350-361.

Marshall, C.P., Carter, E.A., Leuko, S., Javaux, E.J., 2006. Vibrational spectroscopy of extant and fossil microbes: Relevance for the astrobiological exploration of Mars. Vibrational Spectroscopy 41, 182-189.

Marshall, C.P., Love, G., Snape, C., Hill, A., Allwood, A., Walter, M., Vankranendonk, M., Bowden, S., Sylva, S., Summons, R., 2007. Structural characterization of kerogen in 3.4 Ga Archaean cherts from the Pilbara Craton, Western Australia. Precambrian Research 155, 1-23.

McDonald, T.J., Kennicutt, M.C., Rafalska, J.K., Fox, R.G., 1991. Source and maturity of organic matter in glacial and Cretaceous sediments from Prydz Bay, Antarctica, ODP Holes 739C and 741A. Proceedings of the Ocean Drilling Program, Scientific Results 119, 407-416.

Misi, A., Iyer, S.S., Silva-Coelho, C.E., Tassinari, C.C.G., Franca-Rocha, W.J.S., Rocha-Gomes, A.S., Cunha, I.A., Toulkeridis, T., Sanches, A.L., 2000. A metallogenic evolution model for the lead-zinc deposits of the Meso and Neoproterozoic sedimentary basins of the São Francisco Craton, Bahia and Mines Gerais, Brazil. Revista Brasileira de Geociências 30, 302-305.

Moczydłowska, M., 2008. The Ediacaran microbiota and the survival of Snowball Earth conditions. Precambrian Research 167, 1-15.

Nagy, R.M., Porter, S.M., Dehler, C.M., Shen, Y., 2009. Biotic turnover driven by eutrophication before the Sturtian low-latitude glaciation. Nature Geoscience 2, 415-418.

Olcott, A.N., Sessions, A.L., Corsetti, F.A., Kaufman, A.J., de Oliviera, T.F., 2005. Biomarker evidence for photosynthesis during Neoproterozoic glaciation. Science 310, 471-474.

Ourisson, G., Albrecht, P., 1992. Hopanoids. 1. Geohopanoids: The most abundant natural products on Earth? Accounts of Chemical Research 25, 398-402.

Ravizza, G., Turekian, K., 1989. Application of the ^{187}Re-^{187}Os system to black shale geochronometry. Geochimica et Cosmochimica Acta 53, 3257-3262.

Ravizza, G., Turekian, K., Hay, B., 1991. The geochemistry of rhenium and osmium in recent sediments from the Black Sea. Geochimica et Cosmochimica Acta 55, 3741–3752.

Runnegar, B., 2000. Loophole for snowball Earth. Nature 405, 403-4.

Schouten, S., Ossebaar, J., Brummer, G., Elderfield, H., Sinninghe Damsté, J., 2007. Transport of terrestrial organic matter to the deep North Atlantic Ocean by ice rafting. Organic Geochemistry 387, 1161-1168.

Schrag, D.P., Hoffman, P.F., 2001. Life, geology and snowball Earth. Nature, 4096818, 306.

Selby, D., Creaser, R.A., 2003. Re–Os geochronology of organic rich sediments: an evaluation of organic matter analysis methods. Chemical Geology 200, 225-240.

Sherman, L.S., Waldbauer, J.R., Summons, R.E., 2007. Improved methods for isolating and validating indigenous biomarkers in Precambrian rocks Organic Geochemistry 38, 1987-2000.

Suess, E., Balzer, W., Hesse, K.F., Mueller, P.J., Ungerer, C.A., Wefer, G., 1982. Calcium carbonate hexahydrate from organic-rich sediments of the Antarctic Shelf: Precursors of glendonites. Science 216, 1128-1131.

Tuinstra, F., Koenig, J., 1970. Raman spectrum of graphite. Journal of Chemical Physics 53, 1126-1130.

Villanueva, J., Grimalt, J., Cortijo, E., Vidal, L., Labeyriez, L., 1997. A biomarker approach to the organic matter deposited in the North Atlantic during the last climatic cycle. Geochimica et Cosmochimica Acta 61, 4633-4646.

Volkman, J., 2003. Sterols in microorganisms. Applied Microbiology and Biotechnology 60, 495-506.

Yuan, X., Xiao, S., Taylor, T.N., 2005. Lichen-like symbiosis 600 million years ago. Science 308, 1017-1020.

FIGURE CAPTIONS

Fig. 1. Geological map of the São Francisco craton showing sample locality. Inset map shows location of craton in Brazil. Modified from Misi et al., 2000.

Fig. 2. Stratigraphic column based on core log of core MAF 42-88. To the left of the column are the Raman spectra of samples at 858, 783 and 759 m (3 traces) and their GC/MS TIC chromatograms. To the right are the Raman spectra of samples at 817, 816, 812 and 805 m (2 traces) and their TIC chromatograms. The internal standard is marked by a black dot and the *n*-C_{20} and *n*-C_{30} *n*-alkanes are indicated. Raman bands are labeled with their assigned carbon types, as defined in the key.

Fig. 3. (A) Photomicrograph of thin section at 805 m showing organic carbon laminations and pyrite within the black shale unit. NB carbonate nodule in upper right. (B) Enlarged view of another carbonate nodule in black shale unit. Laminations parallel within the nodule are pinched outside the nodule, indicating that the nodule formed early in diagenesis. (C) Photomicrograph of thin section at 759 m, illustrating that the carbonate unit is composed of layers of carbonate and is relatively organic poor.

Fig. 4. Full Raman spectra for samples at 783, 805, 812 and 816 m. NB the sloping baseline in all samples but 783 m, which contains strong D and G

bands. Raman bands are labeled with their assigned carbon types, as defined in the key.

Fig. 5. Selected-ion GC/MS chromatograms from black shale units (in black) and carbonate units (in gray). (A) Partial m/z 191 (hopanes) trace from each meter, shown at the same scale. The *S* and *R* peak assignments define the stereochemistry at C-22, Ts denotes the C_{27} 18α(H),22,29,30-trisnorhopane, Tm denotes the C_{27} 17α(H),22,29,30-trisnorhopane. (B) Partial m/z 217 (steranes) trace from each meter, shown at the same scale. The *S* and *R* peak assignments define the stereochemistry at C-20, while βα, ααα, αββ denote 13β(H),17α(H)-diasteranes, 5α(H),14α(H),17α(H)-steranes, and 5α(H),14β(H),17β(H)-steranes, respectively.

Table 1

H/C ratio values and extract yields

Sample Depth (m)	H/C	Extract yield (μg/g rock)
759	0.65	5.0
783	0.29	7.7
805	0.48	8.1
812	0.68	10.8
816	n.d.[a]	5.8

817	0.56	13.5
858	n.d.[a]	2.4

[a] Not determined.

Figure 1

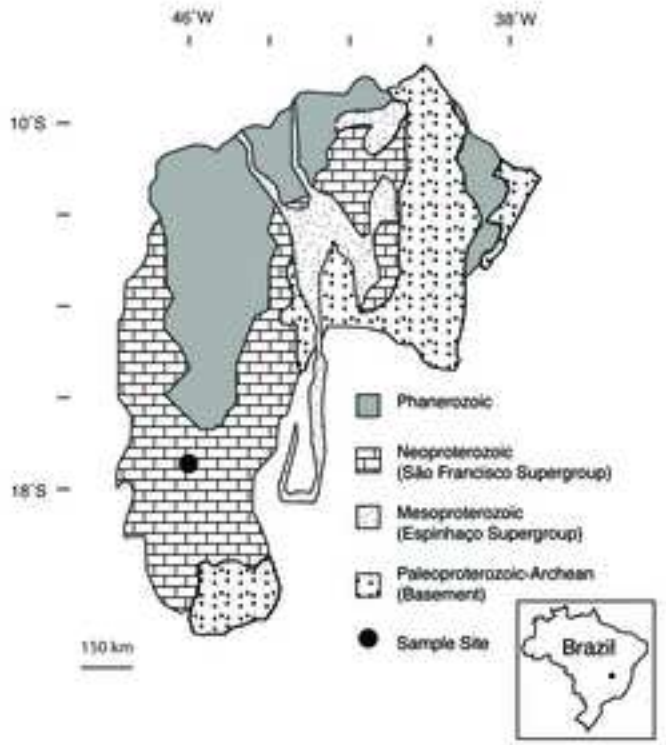

Figure 2

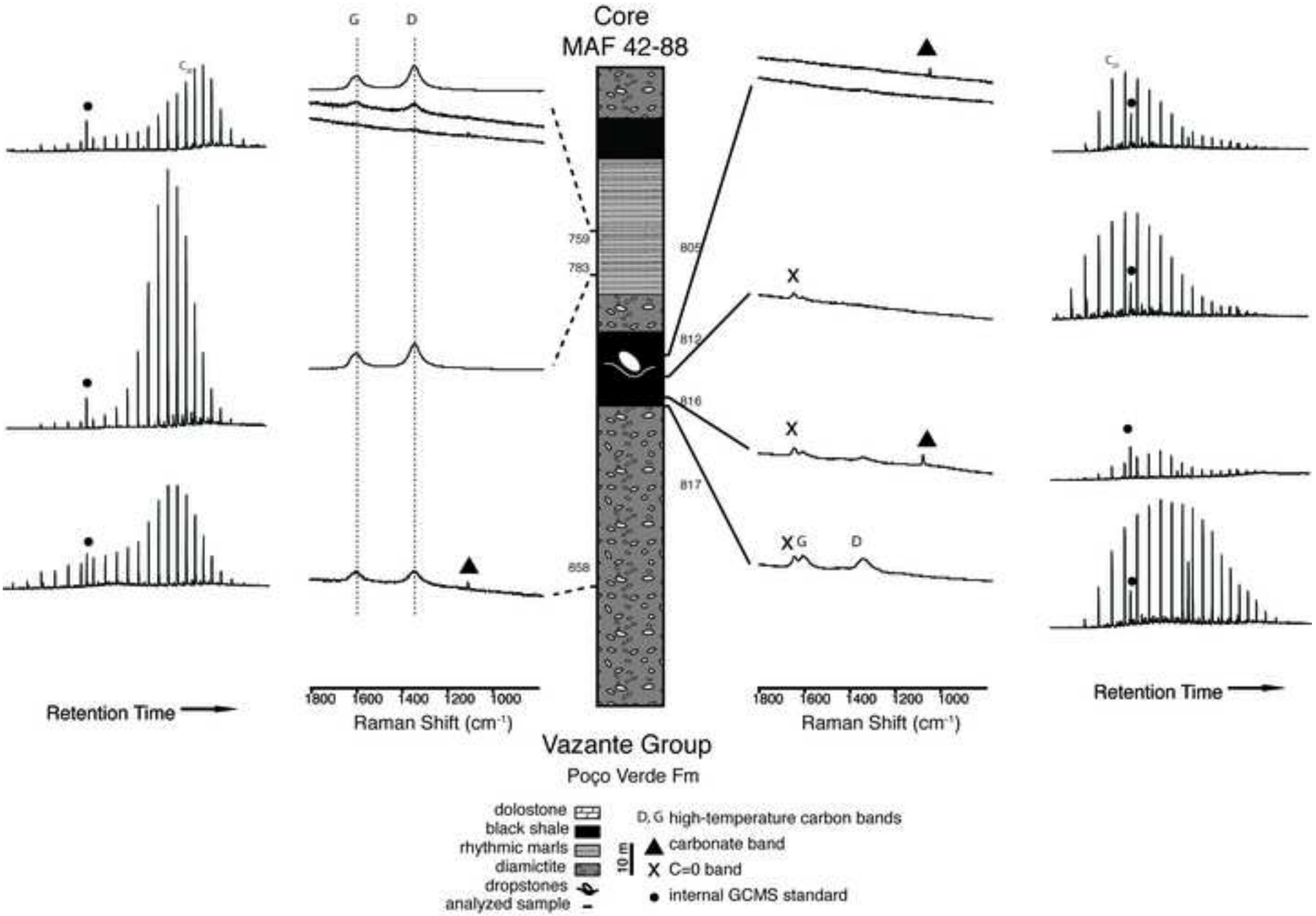

Figure 3

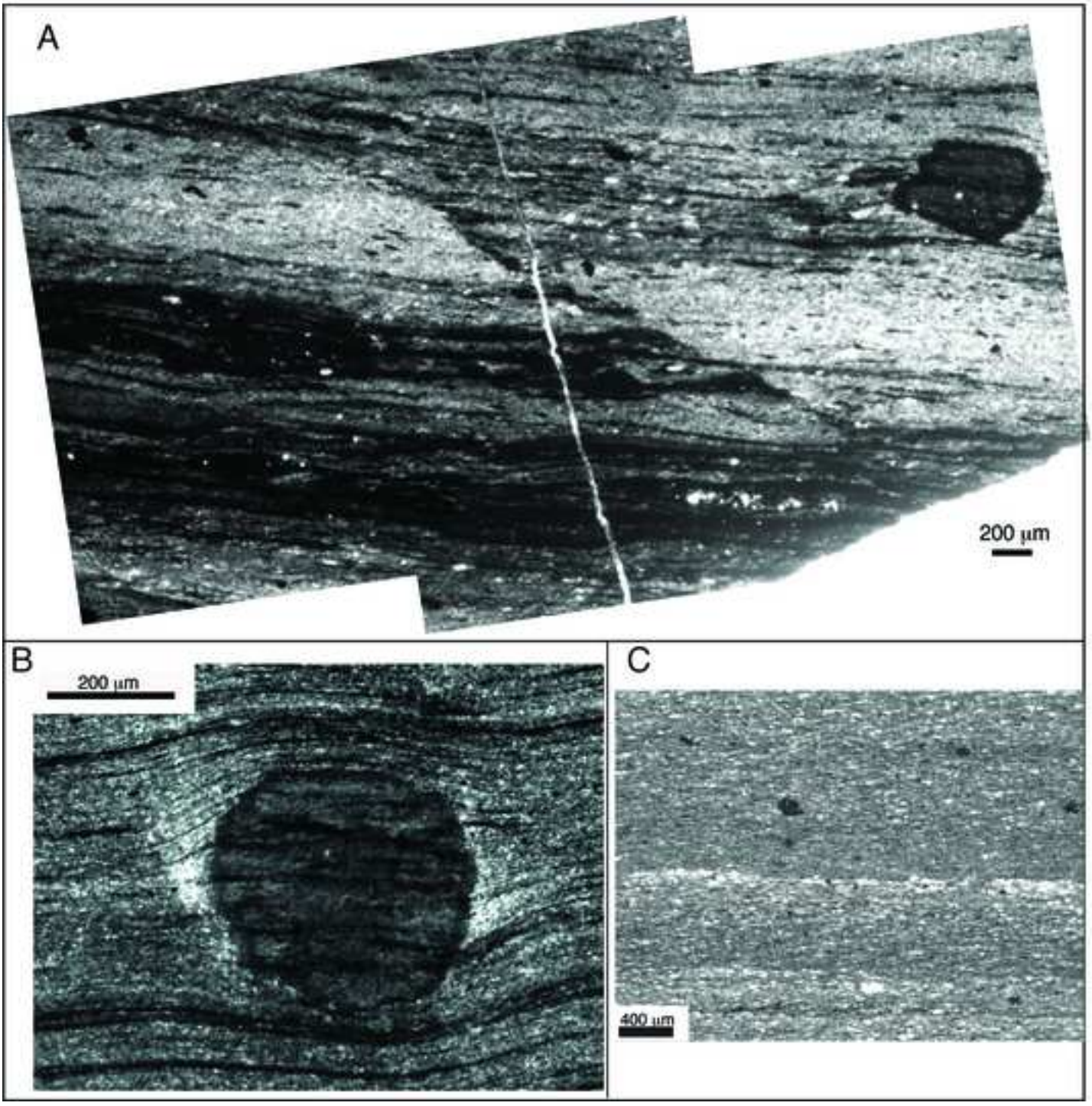

Figure 4

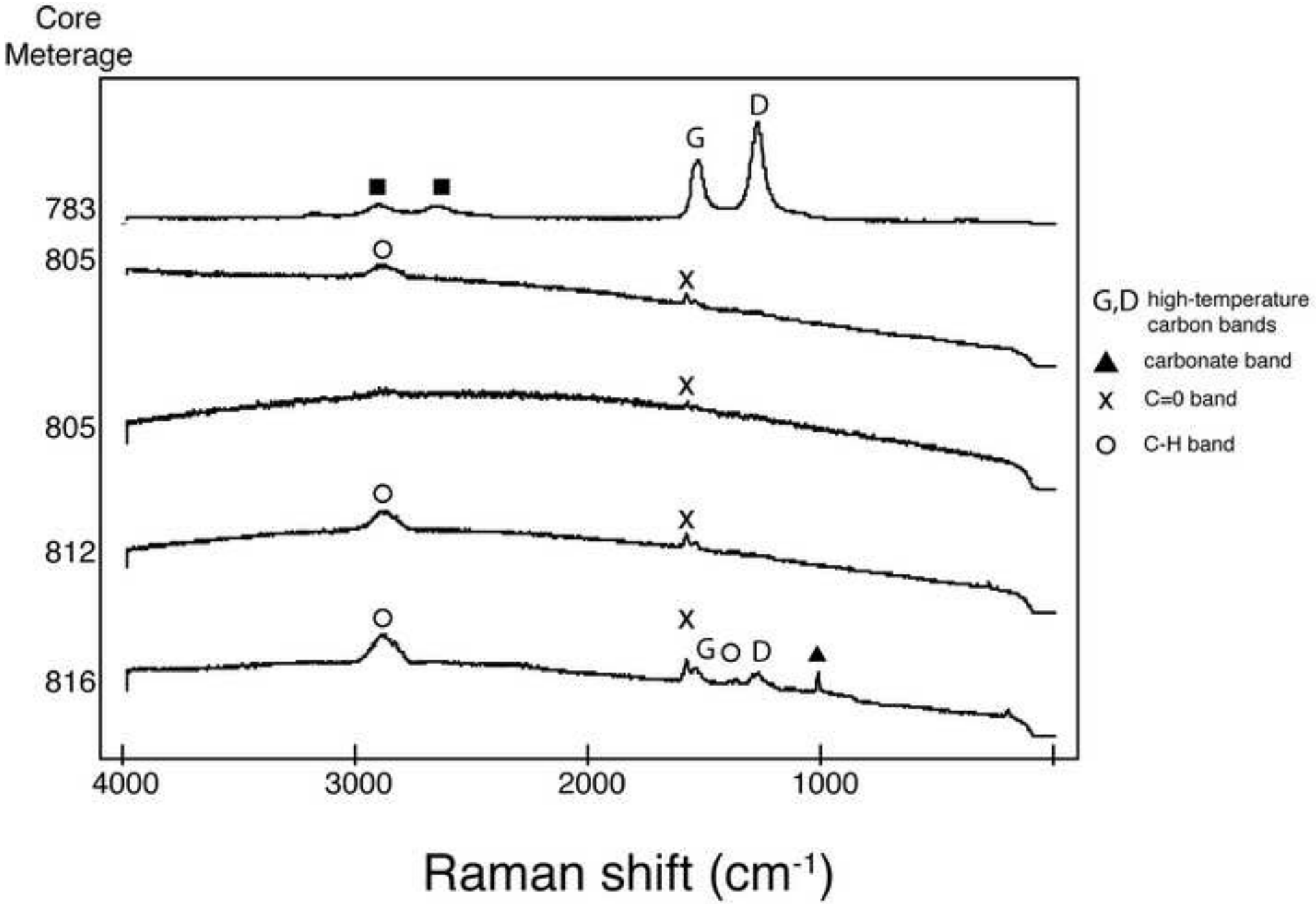

Figure 5